Molecular Imaging by Nanoparticle Bacterial delivery Systems:

R. Sharma
Center of nanomagnetic and Biotechnology, Florida State University, Tallahassee,
FL 32310, Email: rs05h@fsu.edu

ABSTRACT

Dynamic observations have driven the course of imaging biology ever since the first bacterial motility was observed in the late sixteenth century. Continuous imaging of time dependent bacterial motion events is a rapidly emerging biomedical research discipline that extends such observations in living subjects to track the cell trafficking to a more meaningful dimension. Use of paramagnetic properties of nanoparticle may be defined as the visual representation, characterization, and quantification of bacterial processes at the subcellular levels within intact living microorganisms. It is a novel multidisciplinary field, in which the images produced reflect cellular and molecular pathways and in vivo mechanisms of metabolic changes present within the context of physiologically authentic environments. The term “bacterial delivery” and nanobio-imaging” implies the convergence of localized bacterial tracking by using paramagnetic agents sitting inside bacteria using multiple image-capture techniques, basic cell/molecular biology, chemistry, medicine, pharmacology, medical physics, biomathematics, and bioinformatics into a new imaging paradigm.
Keywords: Nanoparticles, bacterial delivery system, imaging

1 INTRODUCTION

1.1 Role of bacteria in biogenic iron oxide formation

Biotic reactions responsible for the formation of biogenic iron oxides include the microbial oxidation of Fe(II) to Fe(III) by a wide range of microorganisms under both acidic and neutral pH and oxic and anoxic conditions. Iron oxide formation also occurs as a result of passive reactions, whereby in situ chemical conditions favour the precipitation of the minerals on biological surfaces, namely bacterial cell walls and extracellular material. These reactions are considered passive because the microbes do not gain energy from the oxidation and nucleation processes, but simply act as binding and nucleation surfaces. The pH changes triggered by microbial metabolic activity and the production of certain bacterial exudates might also favour Fe-oxide formation.

1.2 Magnetotactic bacteria (or **MTB**) are a class of bacteria discovered in the exhibit the peculiar ability to orient themselves along the magnetic field lines of Earth's magnetic field. The term magnetotaxis has been coined to describe the biological phenomenon upon which these microorganisms tend to move in response to the magnetic characteristics of the environment.

Magnetotactic bacteria produce their magnetic particles in chains, as is clearly visible in this microscopic image of *Magnetospirillum magneticum*. The magnetic dipole of the cell is therefore the sum of the dipoles of each BMP which is then sufficient to passively orientate the cell and overcome the casual thermal forces found in a water environment. In the presence of more than one chain, the inter-chain repulsive forces will push these structures to the edge of the cell, inducing turgor and light emission. A unique example of Escherichia coli was reported in cancer real-time imaging. Noninvasive Real-time Imaging of Tumors and Metastases was Tumor-targeting bacteria.

2 Examples of bacteria based imaging

2.1 E. coli and Salmonella based optical imaging

These bacteria accumulate in tumor. Chemotherapy can be localized using bacteria response in tumor. Early observations were to test their microbial activity in tumor. Other anaerobic Clostridium species could proliferate extensively in only hypoxic and necrotic regions of some tumors, whereas they would not grow in well-oxygenated normal tissues. However, facultative anaerobes such as Escherichia coli and Salmonella spp. also localize to transplanted tumors and necrotic areas of the tumor. Attenuated Salmonella typhimurium inhibited the tumor growth and metastasis but remains less understood. Light-emitting microorganisms including E. coli, *Salmonella typhimurium*, *Vibrio cholerae*, and *Listeria monocytogenes* were reported their expressing luciferase (Lux) or green fluorescence protein (GFP) have been used to target and visualize tumors in mouse models. E. coli maintain a stable light signal in the absence of external selection with vivo preclinical imaging potential as shown in Figure 1.

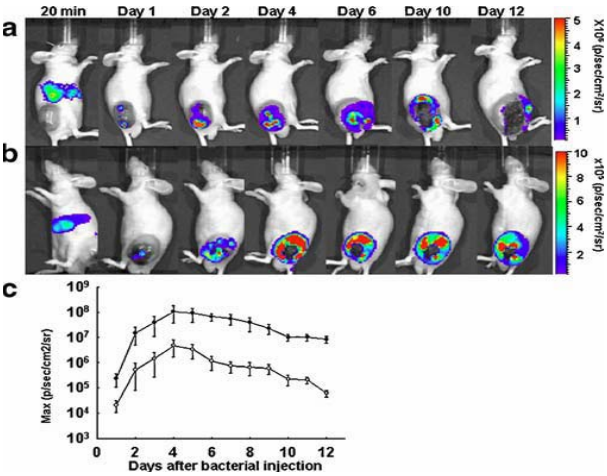

Fig. 1. Distribution of E. coli carrying either pLux or Asd+ pLux in nude mice with orthotopic CT26 colon cancer. In vivo bioluminescence imaging was performed on a nude mouse with CT26 mouse colon cancer in the right lateral thigh. 1_108 E. coli MG1655 pLux (a) or E. coli HJ1020 Asd+ pLux (b) were injected intravenously via the tail vein. The Y-axis indicates photons. c Photon intensity in the tumor region was plotted as a function of time for E. coli pLux (open circles) or Asd+ pLux (closed circles). The ROI was selected manually over the tumor region, and the area was kept constant. Photon intensity was recorded as a maximum [reference 1] within a ROI. The means and SEM were determined from three independent experiments.

2.2 Systemic injection for detection of adenocarcinomas of the gut by PET imaging.

In another series of experiments, PET imaging tested the digestive tumors of the above-mentioned mouse models could be reached by STxB-coupled contrast agents after i.v. administration. For it, PET imaging was used. STxB was chemically coupled to a recently described [^{18}F]fluoropyridine-based maleimide reagent. Using mass spectroscopy, it was observed that all B-chains of the STxB/Cys pentamer were modified, and the functionality of the coupling product was confirmed by cellular trafficking assays. Mice were imaged between 1 and 2 hours after retro-orbital injection of [^{18}F]fluoropyridine-STxB. In all cases, the bulk of radioactivity was found in the urinary tract as shown by the high levels of radioactivity in the bladder and kidneys(see Fig 3). Uptake was also observed in the spleen, lungs, and, to a lesser extent, in the liver. In wild-type mice, the abdominal region was devoid of labeling. In contrast, coronal sections of microPET images (15-minute frame duration) of a 16-month-old tumor-bearing APC mouse at 60 minutes after i.v. injection of ^{18}F-labeled imaging agent for excellent contrast, coronal sections of microPET images (15-minute frame duration) of a 16-month-old tumor-bearing APC mouse at 60 minutes after i.v. injection

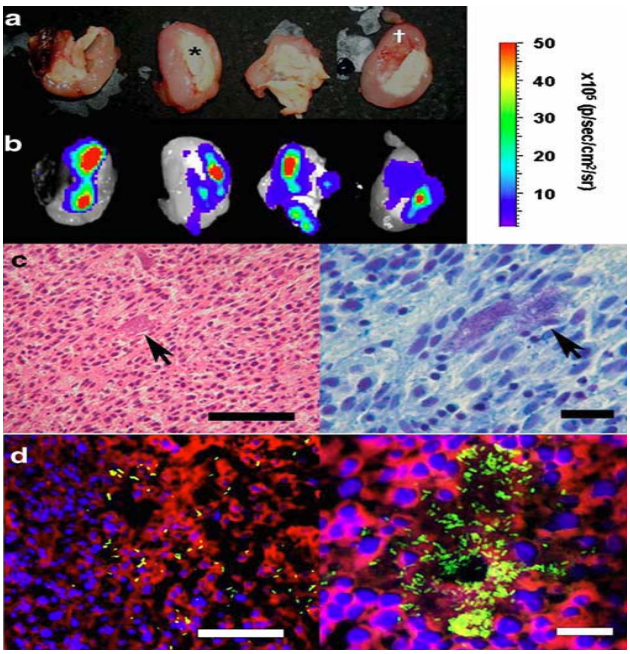

Fig. 2. Distribution of E. coli in tumor tissues. a and b Cross sections of grafted CT26 colon cancer from nude mice after injection of E. coli Asd+ pLux were made at 7 dpi. a and b show cooled CCD bright field and bioluminescence images from the same cross section, respectively. The Y-axis indicates photons_105Isj1Icmj2Isrj1. In a, the central necrotic and peripheral proliferative areas are marked with an asterisk and a cross, respectively. c and d Microscopic localization of E. coli pGFP in tumor tissue. c Bacterial colonies were stained and visualized in subcutaneous CT26 tumor. Left, hematoxylin and eosin (H&E) staining at _200 magnification (bar = 150 mm). Right, Gram staining at x400 magnification(bar = 50 mm). Arrows indicate bacterial colonies. d GFPexpressing E. coli (green) were visualized under confocal microscopy after staining with Texas red (actin, red) and DAPI (nuclei, blue). Left, x600 magnification (bar = 60 mm). Right, _1,200 magnification (bar = 20 mm).

of ^{18}F-labeled STxB showed a high level of STxB uptake at two sites of the digestive tract. The continued capacity of STxB to target the tumors after multiple injections suggests that even if an immune response was raised against STxB, it did not prevent STxB from reaching the tumors. The mouse was then sacrificed and the presence of tumors at the expected sites, the periampullar area (*red arrow*) and one in the lower right abdomen (*green arrow*), was confirmed visually (Figure 3). Gb_3 extraction and overlay allowed to ascertain that both tumors indeed expressed Gb_3. Prognosis of colorectal carcinoma is mainly based on local invasion and distal dissemination, with a 5-year survival of <10% when metastases are present. The Donowitz group has recently described the expression of Gb_3 by metastatic human colorectal carcinomas (10). As a target, Gb_3 may thus allow detection of metastasis by noninvasive imaging approaches, such as STxB-based PET imaging, as described in this study.

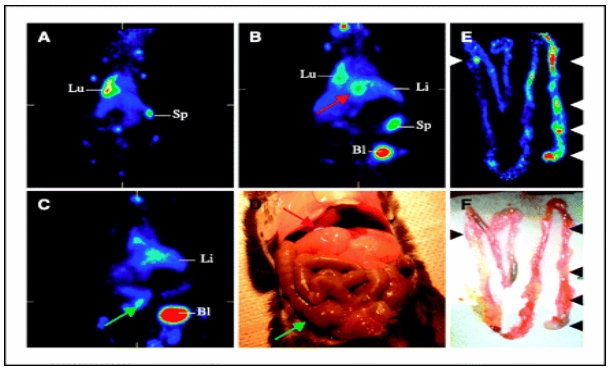

Figure 3. MicroPET coronal images of wild-type and transgenic mice 60 minutes after i.v. injection of 14.8 MBq of [^{18}F]STxB. *A*, in the wild-type mouse, no labeling was detected in the abdominal region. *B* and *C*, on two coronal sections of a transgenic animal (mouse 548), strong labeling was observed in the *top* (*B*, *red arrow*) and *bottom* (*C*, *green arrow*) parts of the digestive tract. For three-dimensional reconstructions of images obtained from mice shown in (*A*-*C*). *D*, the mouse was sacrificed and tumors in the periampullar area (*red arrow*) and the lower abdominal area (*green arrow*) could be detected in the opened abdomen. *E* and *F*, the intestine extracted postmortem from another mouse immediately after [^{18}F]STxB PET showed the optical presence of tumors (*F*) at the same sites where the radioactivity uptake was detected (*E*). Secondary sites of accumulation: *Bl*, bladder; *Lu*, lung; *Li*, liver; *Sp*, spleen [2].

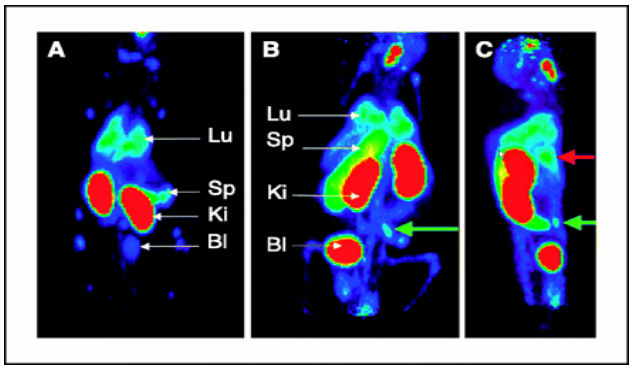

Figure 4. Views from different angles of projection images reconstructed from whole-body data sets of PET acquisitions. These views depict the three-dimensional distribution of the tracer in terms of radioactivity concentrations in mice organs 2 hours after injection of a tracer dose of ^{18}F-labeled STxB. *A*, control mouse from Fig. *A* seen from its ventral side. *B*, tumoral mouse from Fig. *B* and *C* and Film 3 seen from its ventral side. *Green arrow*, tumor in the lower abdomen. *C*, same mouse as in (*B*) and in Fig. *B* and *C* and Film 3, seen from its right side. *Green arrow*, the same lower abdomen tumor shown in (*B*); *red arrow*, a periampullar tumor[2].

Indeed, the PET experiments showed the capacity of ^{18}F-labeled STxB to accumulate in tumors after systemic administration. Cancer staging with PET is currently done with [^{18}F]fluorodeoxyglucose, a biomarker of glucose consumption, which produces contrast because it accumulates more readily in highly metabolically active tumoral cells than in normal tissue. STxB may offer an interesting alternative to [^{18}F]fluorodeoxyglucose in cases where the uptake of this tracer by tumors is low or produces little contrast or false positive because of the presence of metabolically active nontumoral cells, and help circumvent some current limitations of [^{18}F]fluorodeoxyglucose in colorectal and other cancers.

2.3 Magnetic Resonance Imaging

Development of novel MRI contrast agent for cancer tissue with limited toxicity to normal tissues is a challenge. Genetically modified strains of bacteria, such as *Salmonella typhimurium*, has been shown to accumulate at tumor sites. Magnetic Resonance Imaging (MRI) technology has grown over the recent years to become one of the most practiced techniques for imaging. It is capable of showing different characteristics of the imaged tissue. It utilized the difference of levels of magnetization of the tissue subjected to a specific signal. The levels of magnetizations are presented as different contrasts. The new technology of producing high steady magnetic fields enabled the accurate characterization of pathological areas with high resolution.

Multifunctional superparamagnetic nanoparticles offer abundant attractive possibilities in medical imaging [1–5]. One such MRI approach is intravenously administering superparamagnetic nanoparticles in vicinity of tumor tissue and monitoring the tumor uptake of these particles by measuring the regional transverse MRI relaxation rate R_2^*. The enhanced R_2^* of superparamagnetic particles can thus provides an imaging biomarker for tumor tissue. Other benefit is tumor blood volume measurement from absolute change in tumor R_2^*. Engineered non-virulent strains of *Salmonella typhimurium* accumulate and grow selectively to inhibit the growth of primary and metastatic tumors following intravenous injection into tumor-bearing mice. One strain of the bacteria (VNP20009), are highly attenuated and genetically stable. The combination of the lipid mutation and the purine auxotrophy attenuate the virulence of the bacteria by greater than 10000-fold.

We opted to synthesize magnetic nanoparticles with size distribution less than 25 nm and potentially can be utilized as contrast agent in-house development of magnetic nanoparticles.

Next approach was to impregnate the magnetic nanoparticles in attenuated strain of bacteria. *Salmonella* strains such as YS1646 (synonymous to VNP20009) with stable msbB deletion (Vion Pharmaceuticals Inc., New Haven CT) and 10,000 fold activity. This strain of bacteria was administered intravenously to mouse bearing tumors and was shown to accumulate preferentially within the tumors with tumor to normal ratios of 300-25,000:1 and persists in tumor tissue for more than 4

weeks. VNP20009 is sensitive to a number of antibiotics and can be eliminated from the body.

The magnetic nanoparticles have affinity to microorganism but impregnated wild bacteria or attenuated bacteria strains with nanoparticles (naked or encapsulated) are not available. Three modes of impreganation are known:1.**Cellular diffusion:** Small size particles (less than 10 nm) can infuse into the cellular membrane. Due to the requirement of larger particle size (25-50nm) as hyperthermia agent and contrast agent the diffusion approach remains limited. It remains to characterize the intake limits of the particles. Optical microscopy, SEM and/or TEM microscopy were choice. The attenuated bacteria in culture grown with nanoparticles enhanced the induction phase. Use of a fixative arrested the cells and cells settle as pallet. The pellet can be sliced into thin sections using a micro-tome. Optical and well electron microscopy visualize the level of uploading of particles using direct diffusion; **2. In-take of plasmid coated particles.** The nanoparticles coated with plasmid and placed in the cell culture with the bacteria in upper level evaluates the intake using microscopy and fluorescent labeling of the coated particles. These plasmid- coated nanoparticle bearing bacteria can be prepared by transferring DNA into the bacteria cell either as coated particles or by plasmid insertion; **3: Imaging of prototyped tissue.** Magnetic Resonance Imaging (MRI) technology generates MRI signal based on the difference of magnetization of surrounding protons due to dephasing by nanoparticles in high magnetic fields subjected to a specific radiofrequency pulse sequence. The levels of magnetizations at different gradient levels create MRI image with different contrasts. Achievement of high and steady magnetic fields has enabled the accurate MRI tissue characterization of pathological areas at high resolution. Different types of superparamagnetic particles can be used as contrast agents to enhance the MRI signal. However; most commercially available contrast agents display poor specificity. Utilizing the attenuated bacteria as contrast agent carrier will further improve the needed superior specificity. A model capillary made out of polymeric tubing can be utilized in the feasibility MRI evaluation. Both bacteria loaded with nanoparticles and free bacteria used to be injected into polymeric tubing in the presence of buffer solution. In routine, MRI parameters optimized:

Selection of TE and TR for optimizing contrast: The bacteria loaded with nanoparticles can be discriminated on MRI image by varying TE or TR scan parameters at a time and keeping constant TE 200 msec and TR 500, 750, 1000, 1500, 2000 msec (for T2 weighted) or TR 500 msec and TE 5, 10, 15, 20, 25 msec (for T1 weighted) value. T2-w imaging can generate good contrast between bacteria loaded with nanoparticles tube and free bacteria tube. T1-weighted techniques provide a much higher MRI signal (good for morphometry) than T2-weighted sequences (good for tissue density and contrast). For Magnetic Resonance Microimaging (MRIm) technique Impregnated bacteria are injected into a polymeric tube that prototype a vascular vein, free bacteria are injected in a different tube under the same condition. The tube cap will be tightened down to exactly 11 mm so as to fit snugly in the imaging probe head of a 11.7 T superconducting magnet (35 mm bore). Transverse slices of 1 mm thickness obtained using a select gradient of 4.65 G/cm and readout gradient of 2.40 G/cm. In order to standardize bacterial encapsulated superparamagnetic image contrast, scan parameters typically optimized at TE=30 ms; TR=l500 ms; a 512 x 256 matrix is zero-filled to 2048 x 2048; Number of averages=128 for proton weighted images. Image rendering by VNMR software and an Epson printer are matched with histologic images by using ImagePro software. Acquisition of images *ex vivo* at both 11.7 T utilize a special lab built holder. Pixel resolution will be 512 x 256 matrix size with slice thickness 0.4 mm to get 20 microns high resolution and 0.5 mm^3 volume of interest.

Measurement of relaxivity effects of Salmonella encaged nanoparticles: Longitudinal relaxivity of nanoparticles were measured using a standard 2D inversion-recovery (IR) method. Capillaries tubes filled with defined aqueous nanoparticles-solutions serve as external standards in these experiments. Fitting the IR data exponentially allows calculation of the T1 parameter maps and subsequently relaxivity of the nanoparticles.

^{19}F NMR spectroscopy of Salmonella encaged nanoparticles: ^{19}F is a spin one-half nucleus with 100 % natural abundance and a relatively high sensitivity of 0.83 compared with the proton. Utilizing selective water saturation technique using spin echo pulse sequence, fluorine containing metabolites will be monitored in real-time manner. This approach will serve as metabolic signatures of bacteria. All results are awaited.

3 CONCLUSION

Impregnated nanoparticles in bacterial delivery systems are emerging as imaging tools by optical, PET and MRI methods.

REFERENCES

[1].Janssen KP, Vignjevic D, Boisgard R, Falguieres T et al.Can Res 66, 7230-7236,2006.

[2].Min JJ, Kim HJ, Park JH, Moon S, Jeong JH, Hong YJ, Cho KO et al. Mol Imaging Biol 10:54-61, 2008.